Photoacoustic Impulse Response of Lipid-Coated Ultrasound Contrast Agents

Verya Daeichin, *Member, IEEE*, Marco A. Inzunza-Ibarra, Jordan S. Lum, *Member, IEEE*, Mark A. Borden, *Member, IEEE*, and Todd W. Murray

***Abstract*— The utility of ultrasound imaging and therapy with microbubbles may be greatly enhanced by determining their impulse-response dynamics as a function of size and composition. Prior methods for microbubble characterization utilizing high-speed cameras, acoustic transducers and laser-based techniques typically scan a limited frequency range. Here, we report on the use of a novel photoacoustic technique to measure the impulse response of single microbubbles. Individual microbubbles are driven with a broadband photoacoustic wave generated by a nanosecond-pulse laser illuminating an optical absorber. The resulting microbubble oscillations were detected by following transmission of a second laser as it passes twice through the microbubble. The system could even resolve oscillations resulting from a single-shot. As a proof-of-concept study, the size-dependent, linear impulse response of lipid-coated microbubbles was characterized using this technique. This unique method of microbubble characterization with exceptional spatiotemporal resolution opens new avenues for capturing and analyzing microbubble system dynamics.**

***Index Terms*— Laser-ultrasonics, nondestructive testing, photoacoustics, ultrasound contrast agents.**

I. Introduction

MICROBUBBLES are used clinically as ultrasound contrast agents [1] and are being developed for advanced imaging modes, such as molecular imaging [2], acoustic angiography [3], and super-resolution imaging [4], as well as therapeutic applications, such as gene delivery [5], tissue perfusion augmentation [6], and blood–brain barrier disruption [7]. The ability to simultaneously image and mechanically actuate a microbubble may afford real-time manipulation, which, in turn, may enable improved detection schemes and more precise targeting capabilities. Such advancements require a robust knowledge of the microbubble dynamics as it pertains to size, composition, and local microenvironment.

Previous studies have shown that microbubble response can be captured optically [8], [9] and with ultrahigh-speed imaging [10]. Most of the existing single-microbubble oscillation characterization techniques, whether acoustically or optically probing the microbubble, capture a limited part of the full dynamics [11]. An example is the single microbubble spectroscopy technique in which the amplitude response from multicycle, low-amplitude ultrasound pulses at various frequencies is optically captured [12]. The frequencies are scanned and the responses are processed to construct a resonance curve and fit to a linear model to obtain the microbubble viscoelastic properties. Moreover, multiple acoustic pulses are required to characterize the microbubble dynamics and can lead to changes in morphologies, lipid shedding, or destruction of the lipid shell [13]. Therefore, a technique that uses single pulse excitation would reduce both the number of insonations and lipid effects on the microbubble shell.

To capture the full dynamics of oscillation, a microbubble can be excited with a broadband acoustic impulse, and its radial oscillation measured over the full frequency range [14]. Recently, our laboratory has reported on laser-induced thermoelastic and photoacoustic excitation of single microbubbles [15], [16]. The methods reported thus far require either a frequency scanning approach in which the magnitude of the bubble response is measured as a function of frequency using a lock-in amplifier, or an impulse response approach in which an optically absorbing species is attached to the microbubble shell and the bubble is driven through thermoelastic laser excitation. Ultimately, the frequency scanning approach requires individual measurements over the frequency range of interest thus extending the total measurement time. In addition, the microbubble excitation technique in [15] is nonisothermal and dominated by heat transfer into the gas core that induces volumetric thermal-expansion [17], rather than an acoustically induced oscillation. In this letter, we introduce a nondestructive laser-based technique to drive and capture the impulse-response dynamics of microbubble oscillations without any absorbing species attached to the microbubble surface.

II. Methods

The optical system used in this study is depicted in Fig. 1(a) and described in more detail in [18]. A short laser pulse (0.5 ns pulsewidth, Teem Photonics PNG-M02010-1 × 0) from a microchip laser operating at a wavelength of 532 nm and a repetition rate of 1 kHz was used for the excitation of acoustic waves. The laser pulse was sent through a variable attenuator, reflected from a gimbal mirror to control its position on the imaging plane and sent through a long working distance microscope objective (NA = 0.42) to excite the sample. The maximum optical energy incident on the sample was 45 nJ. A continuous wave detection laser (Cobolt Flamenco) operating at a wavelength of 660 nm was sent through the same objective to probe the oscillations of a single microbubble. The sample mount was composed of a mirror located below the

Manuscript received October 5, 2020; accepted January 13, 2021. Date of publication January 18, 2021; date of current version May 25, 2021. This work was supported by the National Institutes of Health under Grant R01CA195051 and the National Science Foundation under Award 1810314. *(Verya Daeichin and Marco A. Inzunza-Ibarra contributed equally to this work.) (Corresponding author: Marco A. Inzunza-Ibarra.)*

Verya Daeichin is with the Department of Imaging Physics, Delft University of Technology, 2628 Delft, The Netherlands.

Marco A. Inzunza-Ibarra, Jordan S. Lum, and Todd W. Murray are with the Department of Mechanical Engineering, University of Colorado Boulder, Boulder, CO 80309 USA (e-mail: marco.inzunza@colorado.edu).

Mark A. Borden is with the Department of Mechanical Engineering, University of Colorado Boulder, Boulder, CO 80309 USA, and also with the Biomedical Engineering Program, University of Colorado Boulder, Boulder, CO 80309 USA.

Digital Object Identifier 10.1109/TUFFC.2021.3052140

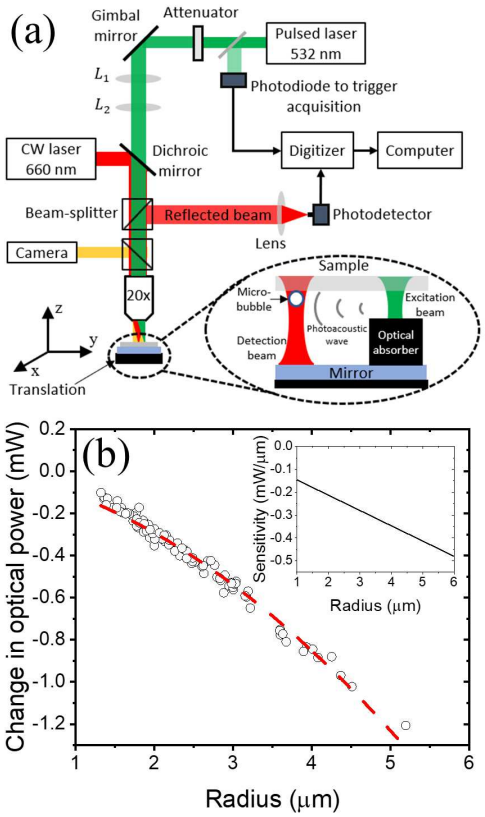

Fig. 1. (a) Experimental set-up used to drive and detect microbubble oscillations. (b) Change in optical power as a function of microbubble radius. A quadratic fit for the data is shown as the dashed-red line. The sensitivity curve ($\partial P/\partial R$) increases linearly with microbubble radius.

imaging plane, a piece of black absorbing tape approximately 3 mm × 3 mm in size (perpendicular to the optical axis) attached to the mirror, and a 270 μm adhesive spacer placed between the mirror and top surface of a coverslip. A dilute concentration of microbubbles (order of 10^6 microbubbles/mL) was injected between the mirror and the coverslip and the detection laser beam was centered on an individual microbubble. After passing through the microbubble, the detection beam reflected from the bottom mirror surface and passed through the microbubble a second time. The scattered light was collected and focused onto a 1-GHz bandwidth photodetector (New Focus, 1601FS-ac). The analog output of the photodetector was amplified by 40 dB and sent to a high-speed digitizer (NI PXIe 5162, 625 MHz sampling frequency). An inline charge coupled device (CCD) camera was used to image the focal plane and size the microbubbles. The uncertainty in the microbubble radius measurement is estimated to be 0.24 μm. Motorized x–y, and z stages controlled the position of the sample and the imaging plane, respectively.

To perform a measurement, the edge of the optical absorber was placed in the field of view of the CCD camera. A single microbubble was then positioned at the center of the detection beam and the excitation beam was steered to the edge of the optical absorber using the gimbal mirror. The microscope was then defocused by translating the sample by 40 μm in the z-direction, such that the spot-size of the detection laser at the microbubble plane was 7.6 μm ($1/e$ Gaussian diameter). Two synchronized shutters near the laser heads were used to control the irradiation timing onto the microbubble and absorber. A partial reflector sent a fraction of the excitation pulse to a photodetector that was used to trigger data acquisition. Absorption of the excitation laser pulse leads to local heating and the generation of a short acoustic pulse through the thermoelastic effect. This pulse propagates from the absorber to the microbubble and drives the microbubble oscillation. Microbubble oscillation produces an intensity modulation of the detection laser probe, and a calibration procedure was used to relate this intensity modulation to microbubble radial displacement following the approach in [15]. In brief, the change in optical power incident on the photodetector with and without a microbubble in the detection beam path is associated with light scattering from the microbubble. This change was measured as a function of microbubble size to obtain the calibration curve shown in Fig. 1(b), and the slope of this curve (inset) provides the sensitivity and allows for the conversion of intensity change to radial displacement.

Microbubble fabrication and sample preparation steps were the same as previously described in [16]. Briefly, the microbubble phospholipid shell consisted of 1, 2-dipalmitoyl-sn-glycero-3-phosphocholine (DPPC) and 1, 2-distearoyl-sn-glycero-3-phosphoethanolamine-N-[methoxy (polyethylene glycol)–2000] (DSPE-PEG2000) at a molar ratio of 9:1 and the gas core was perfluorobutane. Microbubbles were formed by mechanical agitation and were immediately quenched in an ice bath. Centrifugation was used to wash away undesired bubble sizes and residual lipids in the solution [19]. The diluted microbubbles were then injected into the sample mount between the mirror and coverslip. Through buoyancy, the microbubbles floated toward the coverslip where they nonspecifically adhered to the surface [20].

III. Results

Exciting individual microbubbles with a photoacoustic impulse and sensitive laser-based probing provides high enough signal-to-noise to capture the microbubble oscillations with one single-shot. In Fig. 2(a), we demonstrate a single-shot waveform and a corresponding averaged waveform as a function of time (1000 averages) for a single microbubble $R_0 = 2.44$ μm. We also plot the digitally low-pass filtered (10 MHz cutoff frequency) mean response associated with the microbubble radial oscillations. We note that the mean response was used in the signal processing to determine the microbubble viscoelastic properties. In the early part of the averaged waveform, a high-frequency impulse is visible and this is attributed to the photoacoustic wave passing through the detection laser probe. The photoacoustic signal causes a change in the refractive index of the liquid, and scattering of the detection probe from these refractive index fluctuations leads to the observed intensity modulation. Full characterization of the photoacoustic driving signal is beyond the scope of this work. We note that other pulsed lasers could be used in this setup and we would expect similar results so long as the pulsewidth is sufficiently short to generate photoacoustic signals to excite the microbubbles over the bandwidth of interest. To test the linearity of the microbubble radial oscillations, the peak-to-peak amplitude of the microbubble response was measured as a function of incident energy, as shown in Fig. 2(b). For this microbubble, the maximum radial excursion was less than 25 nm from its resting radius or $R/R_0 = 1.01$.

Measurements were performed for multiple microbubble radii ranging from 1 to 5 μm to demonstrate the utility of this technique for single microbubble characterization. For all measurements, the absorber adjacent to the microbubbles was excited with constant energy of 40 nJ. From a Lorentzian

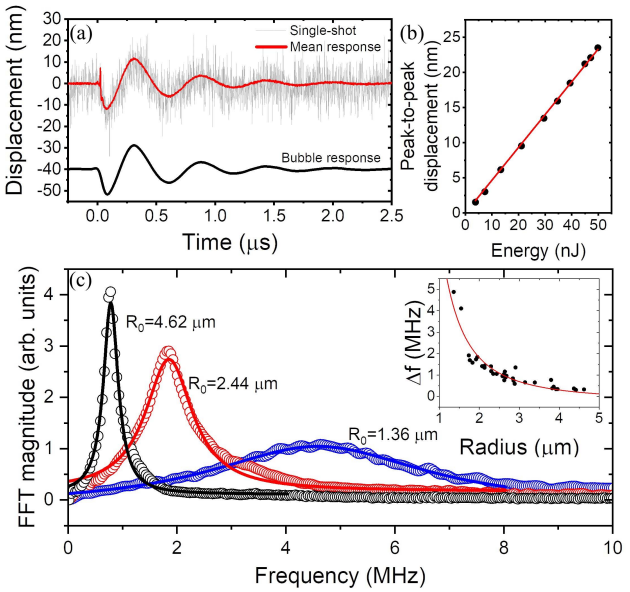

Fig. 2. (a) Microbubble radial displacement ($R_0 = 2.44$ μm). Detected single-shot and corresponding mean response (1000 averages) plotted as a function of time. Also shown in black is the low pass filtered bubble response. The signal is dc offset by 40 nm for visual clarity. (b) Peak-to-peak radial displacement of the same microbubble in (a) with an adj. $R^2 = 1$. (c) FFT magnitude of the mean response for different bubble radius shown as the circles along with a Lorentzian distribution least-squares fit.

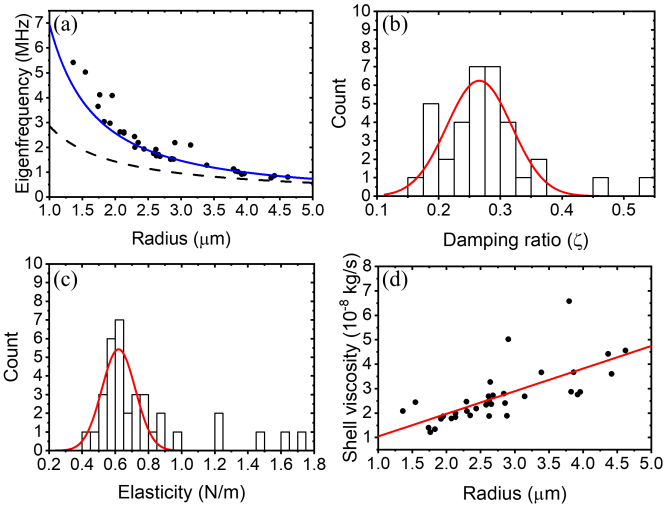

Fig. 3. (a) Experimental results showing eigenfrequency of 35 microbubbles as a function of bubble radius and the theoretical eigenfrequencies for the average shell elasticity $\chi = 0.62$ N/m as the blue solid line. Also plotted as the dashed line for unshelled bubbles. (b) Histogram of damping ratio $\zeta = \Delta f/2f_d$, where Δf is the FWHM of the resonance curve. Mean and standard deviation of the histogram are 0.27 and 0.11, respectively. (c) Histogram of shell elasticity χ (N/m). Line is a Gaussian distribution fit with mean and standard deviation of 0.62 and 0.20 N/m, respectively. (d) Shell viscosity as a function of radius. The linear fit is $y = 9.25 \times 10^{-9} R_0 + 1.23 \times 10^{-9}$ (adjusted $R^2 = 0.49$).

least-squares fit to the time response fast Fourier transform (FFT), we obtain the damped resonance frequency (f_d) from the peak as well as the damping ratio $\zeta = \Delta f/2f_d$, where Δf is the full-width-at-half-maximum (FWHM) of the resonance curve. Shown in Fig. 2(c) are representative frequency-response curves for microbubbles of resting radius R_0 equal to 1.36, 2.44, and 4.62 μm. The inset is the Δf plotted versus radius. Overlaid to the Δf versus radius plot is a fit that is inversely proportional to the square of the radius ($p < 0.05$). As expected, the ringing bandwidth Δf decreases nonlinearly as the microbubble radius increases. For nanometer scale radial oscillations a microbubble behaves as a linear harmonic oscillator [21], and the eigenfrequency of an impulse-driven oscillator is expressed as $f_0 = f_d/(1-\zeta^2)^{1/2}$.

In Fig. 3(a), we demonstrate the experimental results for the eigenfrequency f_0 as a function of microbubble radius. Shell elasticity (χ) was calculated from the linearized form of the modified Rayleigh–Plesset models [22]–[24], which describes coated microbubbles undergoing small-amplitude radial oscillations [12]. Shell elasticity is given as the equation [20]

$$\chi = 1.5\pi^2 f_{\text{measured}}^2 \rho_L {R_0}^3 - 3\kappa P_0 R_0/4 - (3\kappa - 1)\sigma/2 \qquad (1)$$

where ρ_L is the density of the surrounding fluid (10^3 kg/m^3 for water), κ is the polytropic exponent, P_0 is the atmospheric pressure, and σ is the surface tension of the gas–liquid interface. The surface tension σ was assumed to be zero to satisfy the diffusion of a gas bubble in an over-saturated medium [25]. The value for κ was computed for each microbubble measurement following Lum *et al.* [26] and ranged from 1.042 to 1.051. The expression in (1) compensates for the $\sqrt{2/3}$ decrease in eigenfrequency due to an acoustic effect of the microbubble resting on a rigid surface [12]. Fig. 3(a) also includes the theoretical curve of eigenfrequency for an average shell elasticity, described below. The average shell elasticity for DPPC-coated microbubbles matches well with previous measurements, falling in between those reported in [12] and [15]. The dashed line is eigenfrequencies for that of an unshelled microbubble ($\chi = 0$ N/m) with an interfacial surface tension $\sigma = 0.073$ N/m. We can see the eigenfrequency as a function of radius closely follows the linearized Rayleigh-Plesset-type model [12], [26], specific for spherical oscillations of a microbubble in a free medium.

In Fig. 3(b) and (c), histograms and Gaussian distribution fits for the total damping ratio (ζ) and shell elasticity (χ) are depicted. Interestingly, the data followed a normal distribution with a mean of 0.27 and 0.62 N/m for ζ and χ, respectively. As in [26], the damping terms can be described as $\zeta_{\text{total}} = \zeta_{\text{vis}} + \zeta_{\text{rad}} + \zeta_{\text{therm}} + \zeta_{\text{shell}}$, where $\zeta_{\text{shell}} = \kappa_s/\pi {R_0}^3 \rho_L f_0$. The shell viscosity ($\kappa_s$) shows a significant increase ($p < 0.05$) with radius as shown in Fig. 3(d) though scatter in the data makes it difficult to elucidate the functional form. The increase in shell viscosity with microbubble radius has also been observed in prior studies [12], [27].

IV. Conclusion

In conclusion, we have developed and tested a novel technique to drive and measure the impulse response of single microbubbles. A photoacoustic impulse was used to drive microbubbles into small-amplitude oscillations, which were then tracked as a function of time using light scattering. The ability to probe single microbubbles with high fidelity and sensitivity using nondestructive methods offers a powerful tool for the study of microbubble dynamics. Moreover, this technique can resolve microbubble oscillations from a single-shot response. From the radial oscillations, we have computed the shell elasticity (0.62 N/m) and viscosity (order 10^{-8} kg/s), which are in good agreement with previous studies, giving confidence that this method is suitable to probe microbubble properties. Future work using this technique includes driving microbubbles into nonlinear amplitude oscillations by increasing the laser fluence and measuring associated changes in the viscoelastic shell properties.

REFERENCES

[1] P. Frinking, T. Segers, Y. Luan, and F. Tranquart, "Three decades of ultrasound contrast agents: A review of the past, present and future improvements," *Ultrasound Med. Biol.*, vol. 46, no. 4, pp. 892–908, Apr. 2020.

[2] J. K. Willmann *et al.*, "Ultrasound molecular imaging with BR55 in patients with breast and ovarian lesions: First-in-human results," *J. Clin. Oncol.*, vol. 35, no. 19, pp. 2133–2140, Jul. 2017.

[3] R. C. Gessner, C. B. Frederick, F. S. Foster, and P. A. Dayton, "Acoustic angiography: A new imaging modality for assessing microvasculature architecture," *Int. J. Biomed. Imag.*, vol. 2013, pp. 1–9, Jan. 2013.

[4] C. Errico *et al.*, "Ultrafast ultrasound localization microscopy for deep super-resolution vascular imaging," *Nature*, vol. 527, no. 7579, pp. 499–502, Nov. 2015.

[5] T. Ilovitsh *et al.*, "Low-frequency ultrasound-mediated cytokine transfection enhances T cell recruitment at local and distant tumor sites," *Proc. Nat. Acad. Sci. USA*, vol. 117, no. 23, pp. 12674–12685, Jun. 2020.

[6] J. T. Belcik *et al.*, "Augmentation of limb perfusion and reversal of tissue ischemia produced by ultrasound-mediated microbubble cavitation," *Circulat., Cardiovascular Imag.*, vol. 8, no. 4, Apr. 2015, Art. no. e002979.

[7] Y. Meng, K. Hynynen, and N. Lipsman, "Applications of focused ultrasound in the brain: From thermoablation to drug delivery," *Nature Rev. Neurol.*, vol. 17, no. 1, pp. 7–22, Jan. 2021.

[8] J. E. Chomas, P. A. Dayton, D. May, J. Allen, A. Klibanov, and K. Ferrara, "Optical observation of contrast agent destruction," *Appl. Phys. Lett.*, vol. 77, no. 7, pp. 1056–1058, Aug. 2000.

[9] N. de Jong *et al.*, "Optical imaging of contrast agent microbubbles in an ultrasound field with a 100-MHz camera," *Ultrasound Med. Biol.*, vol. 26, no. 3, pp. 487–492, Mar. 2000.

[10] C. T. Chin *et al.*, "Brandaris 128: A digital 25 million frames per second camera with 128 highly sensitive frames," *Rev. Sci. Instrum.*, vol. 74, no. 12, pp. 5026–5034, Dec. 2003.

[11] B. Helfield, "A review of phospholipid encapsulated ultrasound contrast agent microbubble physics," *Ultrasound Med. Biol.*, vol. 45, no. 2, pp. 282–300, Feb. 2019.

[12] S. M. van der Meer *et al.*, "Microbubble spectroscopy of ultrasound contrast agents," *J. Acoust. Soc. Amer.*, vol. 121, no. 1, pp. 648–656, Jan. 2007.

[13] J.-P. O'Brien, N. Ovenden, and E. Stride, "Accounting for the stability of microbubbles to multi-pulse excitation using a lipid-shedding model," *J. Acoust. Soc. Amer.*, vol. 130, no. 4, pp. 180–185, Sep. 2011.

[14] J. L. Raymond *et al.*, "Impulse response method for characterization of echogenic liposomes," *J. Acoust. Soc. Amer.*, vol. 137, no. 4, pp. 1693–1703, Apr. 2015.

[15] J. D. Dove, M. A. Borden, and T. W. Murray, "Optically induced resonance of nanoparticle-loaded microbubbles," *Opt. Lett.*, vol. 39, no. 13, pp. 3732–3735, Jul. 2014.

[16] J. S. Lum, D. M. Stobbe, M. A. Borden, and T. W. Murray, "Photoacoustic technique to measure temperature effects on microbubble viscoelastic properties," *Appl. Phys. Lett.*, vol. 112, no. 11, Mar. 2018, Art. no. 111905.

[17] A. J. Dixon, S. Hu, A. L. Klibanov, and J. A. Hossack, "Oscillatory dynamics and *in vivo* photoacoustic imaging performance of plasmonic nanoparticle-coated microbubbles," *Small*, vol. 11, no. 25, pp. 3066–3077, Feb. 2015.

[18] T. W. Murray *et al.*, "A new in-line laser-based acoustic technique for pillar bump metrology," *J. Microelectron. Electron. Packag.*, vol. 13, no. 2, pp. 58–63, Apr. 2016.

[19] S. Sirsi, J. Feshitan, J. Kwan, S. Homma, and M. Borden, "Effect of microbubble size on fundamental mode high frequency ultrasound imaging in mice," *Ultrasound Med. Biol.*, vol. 36, no. 6, pp. 935–948, Jun. 2010.

[20] J. S. Lum, V. Daeichin, D. F. Kienle, D. K. Schwartz, T. W. Murray, and M. A. Borden, "Changes in microbubble dynamics upon adhesion to a solid surface," *Appl. Phys. Lett.*, vol. 116, no. 12, Mar. 2020, Art. no. 123703.

[21] T. Leighton, *The Acoustic Bubble*. London, U.K.: Academic, 1994.

[22] L. Hoff, P. C. Sontum, and J. M. Hovem, "Oscillations of polymeric microbubbles: Effect of the encapsulating shell," *J. Acoust. Soc. Amer.*, vol. 107, no. 4, pp. 2272–2280, Apr. 2000.

[23] K. Sarkar, W. T. Shi, D. Chatterjee, and F. Forsberg, "Characterization of ultrasound contrast microbubbles using *in vitro* experiments and viscous and viscoelastic interface models for encapsulation," *J. Acoust. Soc. Amer.*, vol. 118, no. 1, pp. 539–550, Jul. 2005.

[24] P. Marmottant *et al.*, "A model for large amplitude oscillations of coated bubbles accounting for buckling and rupture," *J. Acoust. Soc. Amer.*, vol. 118, no. 6, pp. 3499–3505, Dec. 2005.

[25] P. S. Epstein and M. S. Plesset, "On the stability of gas bubbles in liquid-gas solutions," *J. Chem. Phys.*, vol. 18, no. 11, pp. 1505–1509, Nov. 1950.

[26] J. S. Lum, J. D. Dove, T. W. Murray, and M. A. Borden, "Single microbubble measurements of lipid monolayer viscoelastic properties for small-amplitude oscillations," *Langmuir*, vol. 32, no. 37, pp. 9410–9417, Sep. 2016.

[27] K. E. Morgan, J. S. Allen, P. A. Dayton, J. E. Chomas, A. L. Klibaov, and K. W. Ferrara, "Experimental and theoretical evaluation of microbubble behavior: Effect of transmitted phase and bubble size," *IEEE Trans. Ultrason., Ferroelectr., Freq. Control*, vol. 47, no. 6, pp. 1494–1509, Nov. 2000.